Measuring Sources of Manufacturing Process Variations in Automated Fiber Placement Composites

Siddharth Pantoji[1*], Christos Kassapoglou[1], and Daniël Peeters[1]

[1] Faculty of Aerospace Engineering, Delft University of Technology, Kluyverweg 1, Delft, 2629 HS, The Netherlands
* Corresponding author (s.a.pantoji@tudelft.nl)

Keywords: *robot path inaccuracy, tape lateral movement on the roller, tape width variation, tape compaction*

ABSTRACT

Manufacturing variations in the AFP process are one of the causes of gaps and overlaps. These manufacturing variations can be due to robot inaccuracy, tape lateral movement on the roller, tape width variation or tape compaction. These manufacturing variations result in incorrect position or incorrect geometry of the laid tape. An experimental setup was built to measure and investigate the causes of these manufacturing variations and their relative contributions to gap and overlap defects. This setup consisted of an instrumented AFP head. A laser tracker measured the achieved trajectory of the AFP head. A camera measured the lateral movement of the tape on the roller. Laser line scanners measured tape width before and after layup. Experimental results show that the 99th percentile absolute deviations for each of the four measured sources vary from 0.119 mm to 0.534 mm as compared to the specified tape width of 6.35 mm. Among all the measured sources of variations, lateral movement of the tape on the compaction roller was the biggest contributor to gaps and overlaps.

1 INTRODUCTION

All the latest generation of large airliners have composite parts manufactured using Automated Fibre Placement (AFP). AFP is a suitable process for large composite part production and is expected to continue to be so. Huge backlogs in airliner orders translate to a need for faster manufacturing of AFP composites. The runtime fraction of an AFP cell should be maximized to ensure high production rates. However, utilization time fractions of a real-world AFP cell used for manufacturing the fuselage parts of widebody aircraft show that inspection and rework take up ~35% of the time [1]. This wastage of cell time is strongly linked to various types of AFP defects like gaps/overlaps, puckers, wrinkles, bridging, folds, twisted tows, missing tows, splices, fuzz balls etc. Gaps and overlaps are the most numerous of all these AFP defects. For example, they were found to be more than 57% of all the defects for a representative helicopter part [2]. For typical aerospace AFP composites, there is an allowable magnitude of gaps and overlaps. During the layup, every ply is inspected for defects. If a gap/overlap defect bigger than the allowable is found, it is reworked manually. This reduces the run time of the AFP cell.

An ideal meso-structure for any performance-oriented AFP composite would have the tape laid such that the part has spatially uniform fiber volume fraction and desired fiber orientation. This would result in better mechanical performance and less part-to-part variation. This would require that the tape is laid beside each other and on top of other layers in an orderly and intimate fashion. This means that the tape side edges are in abutting contact with side edges of the adjoining tape. Gaps are produced when the side edges of adjacent tapes do not touch each other whereas overlaps are produced when the edges cross over. This is illustrated in the schematics of Figure 1.

Gaps and overlaps can be classified according to their causes. Some gaps and overlaps occur due to an inherent limitation in tow path generation for parts which have tapes laid in non-geodesic paths. This occurs in flat parts manufactured by fiber steering or in doubly curved parts due to their geometry. Tow paths are often generated by parallelly shifting a reference tow path. Depending on the amount of shift, the part has either gaps, overlaps or a combination of both at locations which can be predicted when the layup is designed before manufacturing starts. This is illustrated in the schematics of Figure 2. Other gaps and overlaps occur due to manufacturing process variations. This class of gaps and overlaps are defects which occur due to incorrect relative placement of the edges of adjacent tapes. This placement can have 2 reasons: one, variation in positioning of the tape and, two, variation in geometry of the tape. This is illustrated in the schematics of Figure 3 where the blue colored rectangle denotes the section of a tape being laid on the substrate. Figure 3 (left) shows the ideal tape placement where the tape being laid is in intimate contact with the adjacent tape. Figure 3 (middle) shows the laid tape which has correct geometry but is in incorrect position. Figure 3 (right) shows the tape which has correct position but has incorrect geometry.

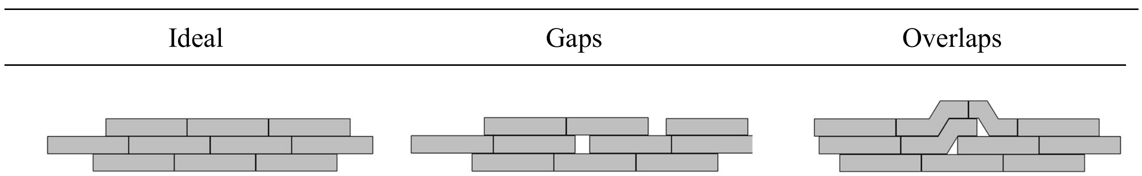

Figure 1: AFP tape layup cross section schematic – ideal AFP composite mesostucture with abutting tapes (left), gaps (middle) and overlaps (right).

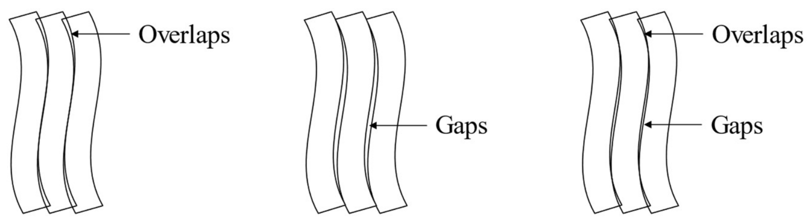

Figure 2: Gaps and overlaps due to shifting of tow path

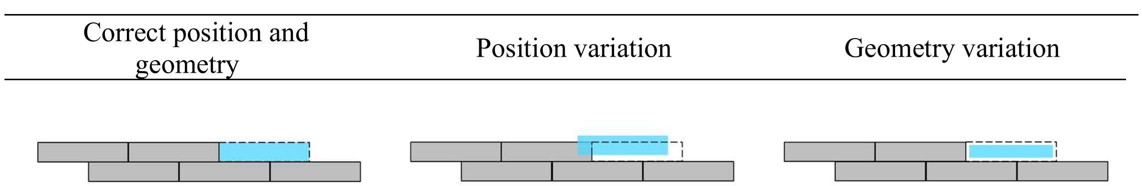

Figure 3: AFP tape layup cross section schematic – ideal tape placement (left), tape placement with position variation (middle), tape placement with geometry variation (right)

Figure 4 shows the further breakdown of these manufacturing process variations into possible sources. Tape position variation could occur due to robot end effector inaccuracy and lateral movement of the tape on the roller. Tape geometry variations could occur due to tape width and thickness variation of the incoming tape or due to tape deformation while being compacted by the roller.

Robot Inaccuracy: AFP robots are programmed to lay down tape on a tool using computer aided manufacturing (CAM) systems. The toolpath defined in the CAM systems is converted into a trajectory of the AFP head by the robot controller. The motion planning involves discretizing the defined toolpath into numerous linear segments, circular arcs or splines [3]. However, there is a difference in the planned toolpath and the achieved trajectory due to geometric, dynamic, thermal and system factors. Geometric factors include inaccuracy of manufacturing of the manipulator parts and deflections due to loads like AFP head weight and process forces. These errors mean that the kinematic equations which relate the robot's joint space and cartesian space, don't do so perfectly. Such errors are expected to be higher in large envelope robotic cells, for example those which make double aisle aircraft components. Dynamic factors like inertial loading and structural resonance can be significant for path-based control [4]. In many robotic applications the end points of the motion need to be accurate. But for AFP systems, the path of the robot during laydown matters. Dynamic factors for an AFP head include the changing weight of the creels as material is expended and reloaded. Another factor is inertial loading. Faster layup speeds are achieved by higher accelerations and decelerations in various phases of the layup cycle. However, this also reduces path accuracy.

Lateral movement of the tape on the roller: The tape feeding system of an AFP system moves tape from the spool to the compaction roller using a system of pulleys and chutes. During the start of each course, tape is extended below the roller before it approaches the tool and presses against it. The cantilever extended tape may not remain straight due to self-weight and residual stresses. This can start the tape at a position moved sideways from its intended position. The tape is under tension as it goes under the compaction roller during layup. This tape tension acts against the lateral movement of the tape. Reduced tension on the tape during some phases of the layup translates to a higher possibility for lateral movement. Steering can also move the tape sideways on the roller due to lateral tractions on the tape.[5]

Tape width variation: AFP systems lay unidirectional tape material available in the form of spools or creels to create large composite parts. This unidirectional tape is manufactured by slitting wider prepregs. However, the widths and thicknesses of slit tape can vary from the specified dimensions. As adjacent tape is laid by the AFP head, less than specified width will cause a gap defect while more than specified width will cause an overlap defect. A tape twist will also lead to width variation causing gap defects.

Tape compaction: During the layup, a heat source raises the temperature of the tape while the compaction roller applies pressure. The heat flux and compaction force values depend on the tape material. For thermoset tapes, the temperature should turn the tape tacky enough for it to stick to the substrate. For thermoplastic tapes being laid with in-situ consolidation, the temperature and pressure should be enough to ensure good ply to ply adhesion and for removing air. These process conditions cause the tape to reduce thickness and increase width. This deformation during layup is seen in higher magnitudes for thermoplastic tapes as compared to thermoset tapes. Thus, this geometry variation in composite tape can create gaps and overlaps [6][7].

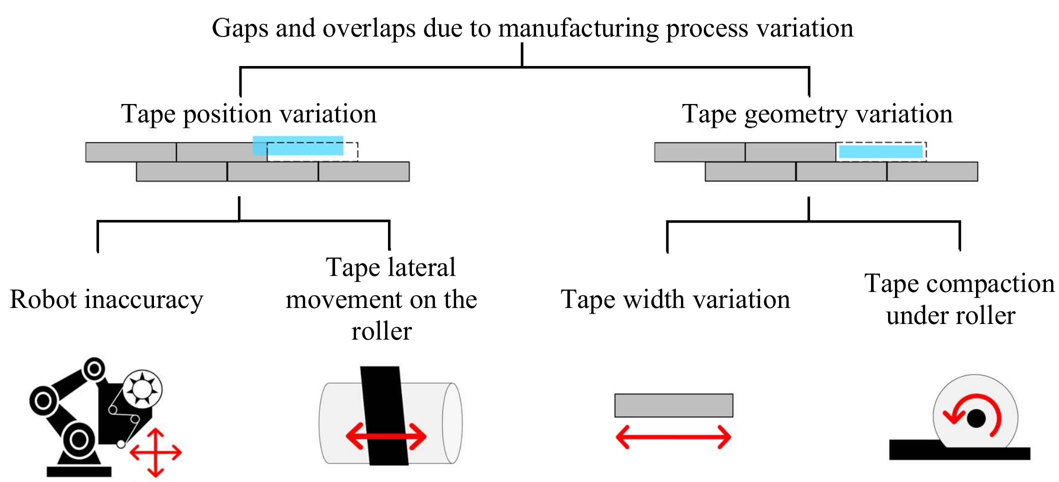

Figure 4: Breakdown of AFP manufacturing process variations which cause gap and overlap defects.

These manufacturing variations act together and result in gaps and overlaps which occur in an AFP composite. Past research work has looked at various aspects of the sources of these manufacturing variations. However, their contribution to gaps and overlaps has not been measured. This work will investigate the relative significance of these manufacturing variations. This will be done by measuring the sources of variations during layup.

2 EXPERIMENTAL SETUP

An experiment was designed to simultaneously measure the various sources of gap and overlap causing manufacturing variations during layup. The measuring system consists of various sensors mounted on an AFP fibre placement head as illustrated in Figure 5.

All the experiments were performed using an AFP system at the robotic cell located at the TU Delft field lab – SAM XL. This system consists of an AFP-XS head made by ADD Composites as the end effector on a KUKA KR 210 R2700 robot manipulator. AFP-XS has a silicone compaction roller with a width of 30 mm and a diameter of 40 mm. It has an infrared heater which increases the tack of the thermoset tape during layup. It can lay down tape with widths of 6.35 mm (¼"), 12.7 mm (½"), 25.4 mm (1") [8]. It is specified to have a maximum layup speed of 1 m/s, a minimum cut length of 85 mm and maximum compaction force of 700N.

The various sensors which make up the measuring system include a laser tracker - Leica AT960 MR, an optical camera - Ximea xiC USB 3.1 Gen1 MC050MG-SY-UB and two laser line scanners (LLS's) – (A) MicroEpilon 2950-25 & (B) MicroEpilon 3060-25. The laser tracker measures the position of the AFP head. The camera views the tape as it goes under the compaction roller. LLS A measures the profile of the tape in the feed system before it reaches the compaction roller. LLS B measures the width of the tape after it has been laid. The laser tracker and the camera give insight into the tape position variation while the two laser line scanners (LLS A & LLS B) give an insight into tape geometry variation. The focus will be on changes in width since these result in defects.

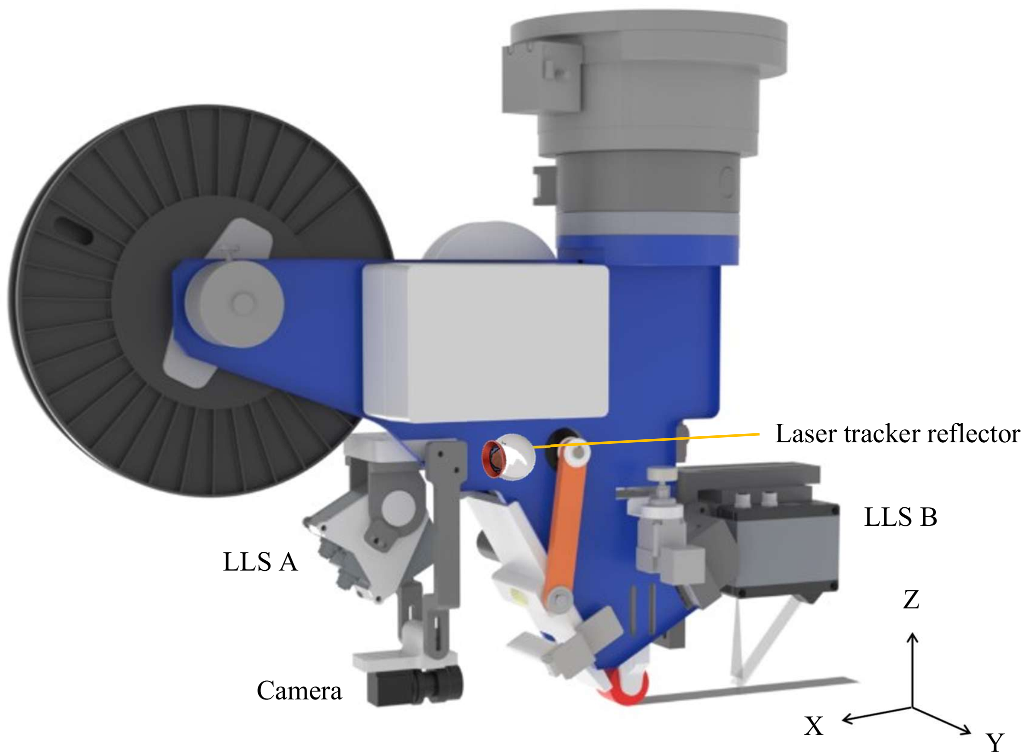

Figure 5: CAD model showing various sensors setup on the AFP head. Layup is in positive X direction.

Mounts for the camera and laser line scanner sensors required for this experiment were custom designed and 3D printed using PLA filament. Being 3-D printed they were relatively faster and cheaper to manufacture over the alternative of CNC milled metal mounts. The mount geometry was designed to rigidly hold the sensors while allowing them to be moved and set in relation to the tape they are observing. Data from the camera and LLS's is collected via USB and ethernet cables routed over the manipulator arm. The retroreflector required for the laser tracker measurements was magnetically attached to a mount/seat which was adhesively stuck to the frame of the AFP head.

The laser tracker is a portable co-ordinate measuring machine (CMM) which uses a reflecting laser beam to measure the targets location and movement. The target is a retroreflector sphere with mirrors. The tracker model used for this experiment uses the Absolute Interferometer (AIFM) method. This along with the azimuth, vertical angles of the beam from angle encoders is used for calculating target's X,Y,Z coordinates in space [9], [10].

The 5 megapixel monochrome optical camera was suitable because it is compact and lightweight. It has a 2464 x 2056 pixel CMOS sensor. The camera is specified to have ambient operating temperature of operation from 0°C to 50°C. It allows for a smaller region of interest to be specified from within the full 2464 x 2056 frame thus allowing for faster frame rates. The camera was paired with a lens which provides manual control on the focal length [11].

The LLS's are 2D profile sensors which were suitable because of their high profile resolution, high profile rate and proven past use in measuring composite tape dimensions [12], [13]. These scanners reflect a line of laser light off the composite tape and use triangulation to measure the profile of the tape. The profile of the tape is output as Y, Z co-ordinates for each measuring point where Z is the measured height at position Y along the laser line. The width of the tape is along Y axis, the thickness is along Z axis while the length of the tape/layup direction is along X axis. MicroEpilon 2950-25 has 1280 measurement points per profile while MicroEpilon 3060-25 has 2048 measurement points per profile. The measurement range for the sensors form a symmetrical trapezoid of average width of 25 mm in the tape width direction and a height of 25 mm and 15 mm respectively in the tape thickness direction. Both sensors allow regions of interest to be defined to measure within fields smaller than the maximum available range to increase the profile rate. The sensors are specified to operate in temperature range of 0°C to 45°C [14], [15].

3 EXPERIMENT AND DATA ANALYSIS

The experiment involved laying down 6.35 mm wide unidirectional thermoset composite tape on a flat plate tool while recording tape position and tape geometry using the above-mentioned sensors. Ten straight line layups of 1 m length were made on the 1 m by 1.5 m rectangular flat tool. The maximum speed was set at 200 mm/s. The robot accelerated after the starting runway phase and decelerated for the stop at tape cutoff. It accelerated again for the end of the layup. These acceleration and deceleration values were set by the black box logic of the robot controller. The 300W IR heater was used at 80% power. Figure 6 shows the program details for each layup. All values are in mm. The straight-line layups were programmed in the X axis direction such that the Y co-ordinate will remain constant for each of them. The layups had Y co-ordinates of 0, 80, 160, 240, 320, 400, 480, 560, 640, 720 respectively. To ensure compaction, the Z co-ordinates for layup were set at -3 such that the tool center point (TCP) moves below the table surface which is at Z = 0. Note that the tool was a steel plate clamp mounted on a measurement table and is not an aerospace grade flat tool.

SpatialAnalyzer application was used to operate and record the position from the laser tracker every 1 ms. The laser tracker has an absolute angular accuracy of ±15 µm + 6 µm/m and an AIFM absolute distance accuracy of ±0.5 µm/m. The tracker was placed approximately 2 m from the tool. The AFP head positions recorded by the laser tracker were that of the achieved trajectory. The difference of the achieved trajectory from the programmed path, in the Y direction is calculated for each recorded set of position co-ordinates. For example, Run 2 had a programmed Y co-ordinate of 80 during layup. One of the recorded data points for position in Run 2 is X = 565.678020, Y = 80.110828, Z = 0.364210. This would mean a deviation of 0.110828 mm from the programmed Y = 80 for that data point.

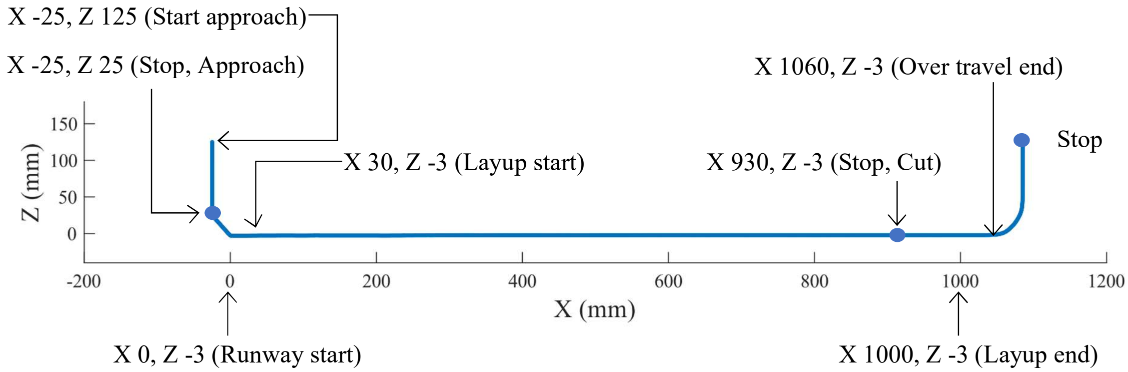

Figure 6: AFP program details

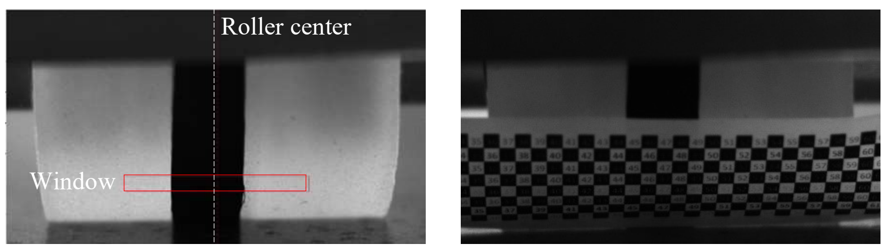

Figure 7: Example frame recorded by the camera. Annotations show the roller center line and the measurement window (Left). Reference image with a checkerboard scale (Right).

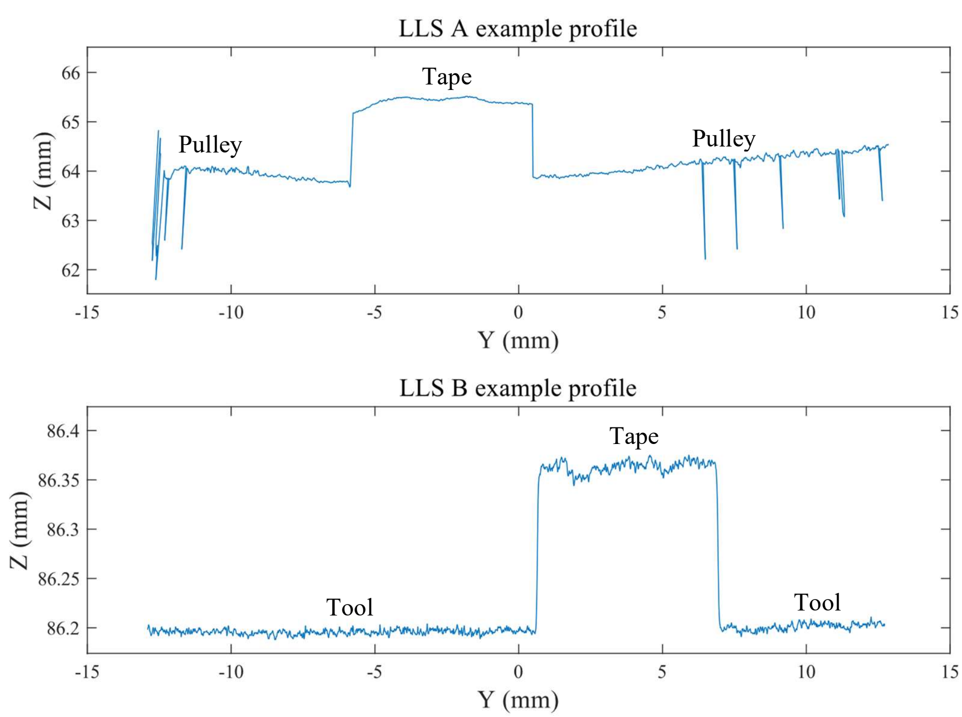

Figure 8: Example profiles measured by the two laser line scanners

The Ximea CamTool application was used to control and operate the camera. To maximize the frame rate, the camera data was acquired by operating it with a region of interest and in a 'free-run' acquisition mode. A region of interest smaller than the full frame could be defined since the camera need not record data from beyond the compaction roller dimensions. The exposure time of the camera was set at 1 ms such that it captures an image which shows the black tape against the white roller with sufficient contrast for a certain heater power setting. This is because heater power also corresponded with illumination of the tape and compaction roller. Higher exposure times not only reduced the frame rate but were seen to increase bright spots of reflections of small surface features of the roller thus negatively affecting image processing required to detect the tape. Sensor resolution in detecting the edge position of a tape was 27 microns. However, calibration of the image processing algorithm allows us to get some interpixel resolution as well. Tape position on the compaction roller was measured using image processing on each recorded frame. Figure 7 shows a red window of size 600 pixels by 50 pixels. This is the region of the frame where the image is the sharpest. The center of the roller is annotated with a dotted red line. Each frame is cropped to the window size and the average intensity of each column of pixels is calculated. The black tape has much lower intensity than the white roller. Thus, the edge of the tape with respect to the center line is calculated by detecting this change in average intensity. This value in pixels is converted to a metric measurement by using a pixel to mm length conversion scale. This scale is obtained from a reference image which has a checkerboard scale whose dimensions are accurately known from its micrograph.

The LLS's were operated using a Python API script. The exposure time of both the LLSs was set at 4 ms such that it reliably captures the tape profile in minimum possible time. LLS A and LLS B have a Y direction resolution of 19.5 microns and 12.2 microns respectively. The maximum Z directional resolution is 2 microns and 1.5 microns respectively. Figure 8 shows example profiles from LLS A and LLS B. The tape edges are found by detecting the sudden change in Z value. The difference between the Y co-ordinate of the two edges is used to calculate width from each such recorded profile. The exposure settings are selected to best view the tape. This means that objects like the feed system or the table in the view of the LLS can be over exposed. Some simple threshold filters are used to remove the aberrant points from each profile.

4 RESULTS AND DISCUSSION

Figure 9 shows the relative frequency distributions for the four measured variations - robot inaccuracy, tape lateral movement on the roller, tape width before compaction, tape width after compaction. The mean and standard deviation are marked in red on the bottom of each distribution. The relative frequency distributions were obtained from measurements from 5 runs. Each run includes laying one meter long tape along a straight line in the X direction. As shown in Figure 4, robot inaccuracy and lateral movement of the tape on the roller are causes of position variation while changes in tape width and tape width after compaction are causes of geometry variation.

4.1 Robot inaccuracy

Figure 9 (A) shows the distribution derived from position measurements of the AFP head from the laser tracker. The data was shifted to have the programmed path centered at 0 mm. Robot position variations have been calculated in the Y direction i.e. the tape width direction. These variations would therefore be an indicator of how the achieved trajectory differed from the programmed path, The distribution appears to be bimodal with a mean of 0.074 mm. The mean is not close to 0 mm, which implies that the position variations are not centered on the programmed path. This means that the achieved trajectory got pushed to one side of the tool. This could be because of the undulation on the table surface or because of the pose of the robot when it is laying tape on the tool. It is also possible that the frequency distribution will converge to a certain shape if values are recorded over a greater number of runs located over the tool in different directions. The range of deviation was 0.604 mm (+0.312 mm to -0.292 mm) which is 9.5% of the specified 6.35 mm tape width.

The measured distribution is for this particular AFP setup and process conditions. The spread of the distribution may increase for robot manipulator with bigger work volumes, heavier AFP heads, faster layups speeds, higher accelerations and decelerations in programmed path etc. The spread of the distribution will decrease for AFP setups which have increased path accuracy of robots due to various strategies such as additional feedback loops, improved kinematic models or robot cell specific compensation [16], [17].

4.2 Lateral movement of the tape on the roller

Figure 9 (B) shows the distribution derived from the tape position measurements made from camera frames. The center of the tape is tracked while the tape is on the compaction roller. These position measurements were made with respect to the roller center line as shown in Figure 7. This roller center position is also annotated on Figure 9 (B). The distribution is an indicator of how the tape moves laterally about its center position on the compaction roller. The distribution has a mean of -0.006 mm which implies that the tape movement is well centered at the center of the roller. The range of deviation was 1.041 mm (+ 0.548 mm to -0.493 mm) which is 16.4% of the specified 6.35 mm tape width. More measurements will be required to determine if the distribution converges to a certain shape. Of the four distributions for various sources of the variations, this distribution had the least samples. This is due to the frame rate limitations of the camera.

It was observed that the tape was moving laterally on the pulleys in the feed system. It then passed through a rectangular metallic chute where the tape has minimal clearance to move. The tape then reaches the roller where it moves laterally as seen in the frequency distribution.

For the straight line layup in this experiment, variables like the tool undulations, roller imperfections and changing tackiness due to variable temperature together resulted in the tape moving laterally on the compaction roller. This spread of this distribution is expected to widen when steering is involved. This steering could be due to curvilinear path on flat tool or non-geodesic paths on doubly curved tools. The spread of this distribution is expected to be narrower for tackier materials and for higher tape tension arising from the spool brake. This is because the tractions in the width direction which cause lateral movements will be opposed by friction forces and a component of the tape tension.

These experiments were done with a single tow AFP setup. However, for multi-course machines, some additional factors will come into play. These include wider compaction rollers, non-uniform heat flux across the width of the roller, more complex tape feed systems, interaction of the multiple tapes with each other etc.

4.3 Tape width variation

Figure 9 (C) shows the distribution derived from geometry measurements of the tape made with a laser line scanner. LLS A recorded profiles of the tape in the tape feed system before it enters the chute leading to the compaction roller. The tape width variation has been recorded by calculating the edge-to-edge distance in each profile. The distribution is an indicator of how the width of the tape varies for the given batch of the unidirectional tape material. The distribution has a mean of 6.345 mm and a standard deviation of 0.058. The mean value is close to the specified tape width of 6.35 mm. Figure 9 (C) shows that a normal distribution can be used to statistically model the width of the tape. The range of deviation was 0.521 mm (6.019 mm to 6.540 mm) which is 8.2% of the specified 6.35 mm tape width.

Of the four measured sources of manufacturing variations, this source had the narrowest spread. This indicates that tape slitting is a well-controlled process for the used brand and specification of unidirectional tape. However, the spread is on both sides of the specified width value. Some tapes are specified to have unilateral tolerance only on the lesser side of specified width. For example, $6.35^{+0.0}_{-0.2}$ mm. This is to prevent overlaps in the layup due to width variation. It is not known if the width deviation for such tapes will also have similar normal distributions.

4.4 Tape compaction

Figure 9 (D) also shows the distribution derived from geometry measurements of the tape made with a laser line scanner. LLS B recorded profiles of the tape after it was laid on the tool. The tape width variation after compaction has been recorded by calculating the edge-to-edge distance in each measured profile. The distribution is an indicator of how the width of the tape varies after it has been compacted by the compaction roller. The distribution has a mean of 6.310 mm and a standard deviation of 0.066.

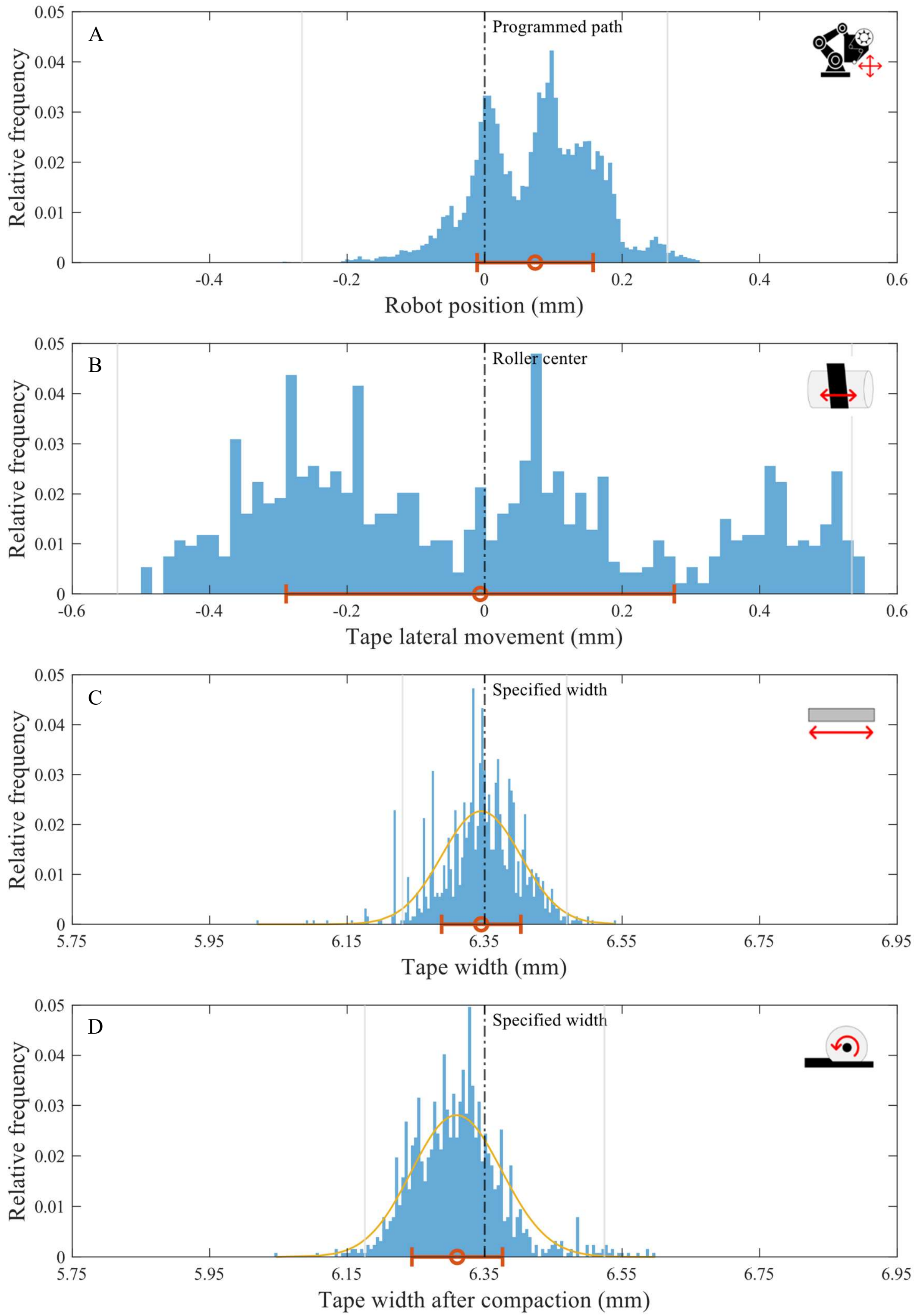

Figure 9: A, B, C, D (top to bottom) Measured manufacturing variations which cause gaps and overlaps. Note that the X and Y axes are equally scaled. Means and ±1σ values are annotated in orange. 99th percentile deviation values are annotated by grey lines. Fits are annotated in yellow.

The mean value of the tape width has reduced after compaction, but the spread has increased. Figure 9 (D) shows that a normal distribution can be used to statistically model the width of the tape after compaction. The range of deviation was 0.552 mm (6.046 mm to 6.598 mm) which is 8.7% of the specified 6.35 mm tape width.

The mean measured width of the tape after compaction was lower than the mean measured width of the tape before compaction. This could be due to two reasons. The width measurement algorithm looks at edge to edge distance. If the tape is curled, its width would be recorded at a value less than its actual width. This indicates a need for an improved algorithm which measures width by measuring the length of the tape profile rather than edge to edge distance. Also, the width measurements are made soon after the tape is laid down. This could mean that transient effects in geometry if any might still be playing out. This indicates that the measurements by LLS B should be re-done after some time to check for these transient effects.

4.5 Combined effect of the measured sources of manufacturing variations

The deviations from the four sources of manufacturing variations in combination lead to the resultant magnitude of the gap/overlap defect. Table 1 shows that one of the sources of variations – lateral movement of the tape on the roller – is a much higher contributor to gap/overlap defects compared to the other three sources. This knowledge can help prioritize future technological improvements in AFP systems.

Typically, thermoset AFP composites have adjacent courses shifted by a value higher than the course width. This is to deliberately cause a gap between adjacent courses and reduce the chances of an overlap. This is because overlaps cause a knockdown in performance while gaps get filled up during the curing cycle in an autoclave. The region near the gaps however have a lower volume fraction [18]. If the probabilities and ranges of manufacturing process variations which cause gap/overlap defects are known, it may be possible to minimize the shift of adjacent courses resulting in more uniform fiber volume fractions.

The 99th percentile absolute deviation for the two sources of position variations are 0.266 mm and 0.534 mm. The 99th percentile absolute deviation for the two sources of width (geometry) variations are 0.119 mm and 0.174 mm. These are annotated with grey vertical lines in Figure 9. These respective deviation values are marked on both sides of the correct value of 0 mm in Figure 9 (A & B) and on both sides of the specified value of 6.35 mm for Figure 9 (C & D).

	Robot inaccuracy	Tape lateral movement	Tape width variation	Tape width variation after compaction
Range (mm)	0.604	1.041	0.521	0.552
Range as Percentage of specified width	9.5 %	16.4 %	8.2 %	8.7 %
Mean (mm)	0.074	-0.006	6.345	6.310
Standard deviation (mm)	0.084	0.282	0.058	0.066
99th percentile deviation (mm)	± 0.266	± 0.534	± 0.119	± 0.174

Table 1: Summary of measured manufacturing variations which cause gaps and overlaps.

Table 1 shows the various statistical descriptors for the four sources of manufacturing variations. By collectively considering the four measured relative frequency distributions, inferences about the frequency and magnitude of gaps and overlaps could be made. Furthermore, if the performance knockdown due to various magnitudes and frequencies of gap/overlap defects is known, distributions of the performance of AFP composites can be obtained. Such calculations can be useful for design and certification activities.

5 CONCLUSIONS

Manufacturing variations cause gap and overlap defects which slows down AFP composites manufacturing and negatively affects mechanical performance. A methodology to measure gap and overlap causing manufacturing variations has been presented and preliminary results were obtained. The manufacturing variations were broken down into two categories depending on if they cause gaps and overlaps due to position variation or by geometry variation. Robot inaccuracy and lateral movement of the tape on the roller are causes of position variation while changes in tape width and tape width after compaction are causes of geometry variation. An experimental setup involving various sensors on an AFP head was implemented to measure the distribution of deviations from each of the sources of manufacturing variations. The 99th percentile absolute deviations for each of the four measured sources – robot inaccuracy, robot lateral movement, tape width variation, tape width variation after compaction– were 0.266 mm, 0.534 mm, 0.119 mm, 0.174 mm respectively. Among all the measured sources of variations, lateral movement of the tape was the biggest contributor to gap/overlap causing deviations. Statistical information from such experiments can be useful in predicting the magnitude and frequency of gap and overlap defects caused by manufacturing variations in AFP composites.

ACKNOWLEDGEMENTS

The authors acknowledge the funding received for the RDM project "liquid hydrogen composite tank for civil aviation", a subsidy from the R&D Mobily sector arrangement from the ministry of economic affairs and climate, executed by Rijksdienst voor Ondernemend Nederland (RVO). With this arrangement RVO contributes to sustainable development goals 8, 9 and 13, commissioned by the ministry of economic affairs and climate. This project helped to set up the experimental infrastructure and data acquisition system.

The authors also acknowledge the support of Daniel Atherstone for the CAD modelling of the sensor mounts.

REFERENCES

[1] T. Rudberg, "AFP 4.0," 2022. [Online]. Available: https://www.electroimpact.com/WhitePapers/AFP4.0.pdf

[2] "SA2GE Project," 2015.

[3] A. M. Mendes Florindo, "LayLa: An open-source offine programming framework for composite deposition," 2020, [Online]. Available: http://repository.tudelft.nl/.

[4] B. Greenway, "Robot accurary," *Ind. Rob.*, vol. 27, no. 4, pp. 257–265, 2000, doi: 10.1108/01439910010372136/FULL/PDF.

[5] S. Rajan, M. A. Sutton, S. Sockalingam, W. McMakin, Z. Gurdal, and A. Kidane, "Simulations and experiments for automated fiber placement of prepreg slit tape: Wrinkle formation and fundamental observations," *Compos. Part B Eng.*, vol. 201, no. January, p. 108287, 2020, doi: 10.1016/j.compositesb.2020.108287.

[6] R. T. D. M. J. P. Jos van Kollenburg, "HOW SMART IS SMART MANUFACTURING?," 2022.

[7] D. Peeters, P. Quenzel, L. Netzband, A. M. Florindo, S. Hesseler, and T. Gries, "Predicting the formation of gaps and overlaps due to width variations of dry-fiber tapes during automated

fiber placement," 2022. [Online]. Available: https://www.medst.rwth-aachen.de/cms/MedST/Forschung/Publikationen/~epcs/Details/?file=844304&lidx=1

[8] ADD Composites, "ADD Composites (Espoo, Finland) website." https://www.addcomposites.com/afpxs (accessed Apr. 20, 2023).

[9] Hexagon, "Leica Absolute Tracker AT960."

[10] Hexagon, "Laser Tracker Fundamentals (11400-00-00)." https://learning.hexagonmi.com/catalog/course.asp?id=16921&cid=6322 (accessed Apr. 20, 2023).

[11] Ximea, "Ximea xiC Camera." https://www.ximea.com/en/products/usb-31-gen-1-with-sony-cmos-xic (accessed Apr. 20, 2023).

[12] D. H. Nguyen, X. Sun, I. Tretiak, M. A. Valverde, and J. Kratz, "Automatic process control of an automated fibre placement machine," *Compos. Part A Appl. Sci. Manuf.*, vol. 168, p. 107465, May 2023, doi: 10.1016/J.COMPOSITESA.2023.107465.

[13] I. Tretiak *et al.*, "REAL-TIME MATERIAL MEASUREMENT FOR AUTOMATED FIBRE PLACEMENT," vol. 2, pp. 25–31, doi: 10.5075/epfl-298799_978-2-9701614-0-0.

[14] Micro-Epsilon, "scanCONTROL 30x0." https://www.micro-epsilon.com/2D_3D/laser-scanner/scanCONTROL-3000/ (accessed Apr. 20, 2023).

[15] Micro-Epsilon, "scanCONTROL 29x0." https://www.micro-epsilon.com/2D_3D/laser-scanner/scanCONTROL-2900/ (accessed Apr. 20, 2023).

[16] K. A. Jeffries, "Enhanced Robotic Automated Fiber Placement with Accurate Robot Technology and Modular Fiber Placement Head," *SAE Int. J. Aerosp.*, vol. 6, no. 2, pp. 774–779, 2013, doi: 10.4271/2013-01-2290.

[17] T. Rudberg, "Increasing Machine Accuracy by Spatially Compensating Large Scale Machines for Use in Constructing Aerospace Structures," *SAE Int. J. Aerosp.*, vol. 6, no. 1, pp. 2013-01–2298, Sep. 2013, doi: 10.4271/2013-01-2298.

[18] W. E. Guin, J. R. Jackson, and C. M. Bosley, "Effects of tow-to-tow gaps in composite laminates fabricated via automated fiber placement," *Compos. Part A Appl. Sci. Manuf.*, vol. 115, pp. 66–75, Dec. 2018, doi: 10.1016/J.COMPOSITESA.2018.09.014.